Synthesis, Structure, and Photocatalytic Activity in Orthorhombic Perovskites LnVO(3) and Ln(1−x)Ti(x)VO(3) (Ln = Ce, Pr, and Nd)

ARTICLE *in* INDUSTRIAL & ENGINEERING CHEMISTRY RESEARCH · AUGUST 2009

Impact Factor: 2.59 · DOI: 10.1021/ie9006134

4 AUTHORS, INCLUDING:

Dipankar Saha
Indian Institute of Science
20 PUBLICATIONS **94** CITATIONS
SEE PROFILE

Sudarshan Mahapatra
Dr. Reddy's Laboratories
17 PUBLICATIONS **190** CITATIONS
SEE PROFILE

Giridhar Madras
Indian Institute of Science
553 PUBLICATIONS **9,877** CITATIONS
SEE PROFILE

Synthesis, Structure, and Photocatalytic Activity in Orthorhombic Perovskites $LnVO_3$ and $Ln_{1-x}Ti_xVO_3$ (Ln = Ce, Pr, and Nd)

Dipankar Saha,[†] Sudarshan Mahapatra,[†] T. N. Guru Row,*[,†] and Giridhar Madras[†,‡]

Solid State and Structural Chemistry Unit and Department of Chemical Engineering, Indian Institute of Science, Bangalore 560 012, India

Orthorhombic perovskite type $LnVO_3$ and $Ln_{1-x}Ti_xVO_3$ (Ln = Ce, Pr, and Nd) have been synthesized by the solid state method. The structures of these compounds have been unequivocally established based on high resolution powder X-ray diffraction data using Rietveld refinement methodology followed by difference Fourier analysis. It is shown that substitution of Ti occurs at the vanadium site and not at the cerium site. The compounds have been tested for photocatalytic degradation of various dyes and substituted phenols. It is observed that doping of Ti remarkably improves the photodegradation efficiency of these orthorhombic perovskites.

Introduction

Perovskites have a general formula ABO_3, where both A and B are in the +3 oxidation state and the "A" cation is larger than the "B" cation. The ideal perovskite structure has a cubic space group *Pm3m-O*$_h$ where A and B cations are 12- and 6-fold coordinated, respectively.[1] The importance of mixed oxides in the area of heterogeneous catalysis has been extensively studied in the last few decades and has been highlighted in several reviews.[2–4] In general, the perovskite structure is viewed as a super structure with a ReO_3 type framework which is identified as a host structure.[5] The importance of synthesizing multicomponent perovskite by selective substitution of cations in A and B positions has been illustrated in the discovery of copper based high temperature superconductors.[6] Further, the consequence of deviations from the ideal structure leads to lower symmetry space groups in rhombohedral, tetragonal, orthorhombic, and monoclinic crystal systems. Such changes result in altered physical and chemical properties involving both surface and bulk characteristics. It is noteworthy that transformation from lower symmetry to high symmetry occurs at elevated temperatures[7] suggesting the robustness associated with perovskites. Nonstoichiometry results in the generation of either cation or anion vacancy. For example, the brownmillerite structures $Ca_2Fe_2O_5$[8] and $La_2Ni_2O_5$[9] show anion vacancy. Oxygen deficient $LaCuO_{3-\delta}$ undergoes phase change from oxygen deficient phase to highly oxidized rhombohedral $LaCuO_3$.[10] Oxygen excess nonstoichiometry is also shown by systems like $LaMnO_{3+\delta}$,[11] whereas $CaTiO_3$ shows oxygen deficiency created by cation nonstoichiometry.[12]

Ternary oxides of transition metals with orthorhombic perovskite type structure exhibit strong correlation involving spin, orbital, and charge leading to a large variety of unusual physical and magnetic properties. In particular, lanthanide orthovanadates of the composition $LnVO_3$ show strong orbital−lattice interaction[13] and orbital-ordering-induced phase transition.[14] $CeVO_3$ exhibits a second order phase transition from the orthorhombic to the monoclinic system at 154 K, and it undergoes an isostructural phase transition at Néel temperature (T_N = 134 K). While $PrVO_3$ shows a similar temperature dependent magnetization behavior,[15] $SmVO_3$ and $NdVO_3$ show N-type ferrimagnetic properties.[16–19] Recently, it has been shown that substitution at A and B sites by aliovalent cations generate materials with specific applications.[20] For example, $La_{1-x}Ca_xVO_3$ is a thermoelectric material, whereas $CeTi_{0.5}V_{0.5}O_3$ shows spin glass formation at lower temperatures due to random occupation of Ti and V at the same crystallographic site.

Photocatalytic degradation of dyes and organics is of fundamental importance in wastewater treatment, cleanup of oil spills, and other related problems of environmental interest.[21] Several factors like band gap energies, features associated with cation vacancy, oxygen deficiency, and surface area influence the performance of materials used in photocatalytic degradation.[22] Substituted $LnVO_3$ materials serve as excellent semiconductor oxides for such studies as they are stable over prolonged periods of time and possess suitable band gaps (E^0 = 2.8 eV).[21] Perovskite compounds have been used for heterogeneous catalysis like CO oxidation, oxidation of hydrocarbons, NO_x decomposition, and exhaust treatment.[7] Compounds like $SrTiO_3$[23] and $KTaO_3$[24] have been used for photocatalytic splitting of water. In addition, titanates and cobaltites have been extensively used for photocatalytic oxidation of CO[25,26] and photocatalytic synthesis of ammonia with $SrTiO_3$ as a catalyst.[27]

The objective of this study is twofold. First, the synthesis of $LnVO_3$ and Ti substituted $LnVO_3$ has been carried out followed by structure determination by using a unique approach of combining Rietveld refinement with difference Fourier analysis. This methodology clearly indicates the presence of titanium at the vanadium site. Second, the photocatalytic activity of these compounds has been studied which indicates that these compounds are specific in degrading chloro/nitro-substituted phenols.

Experimental Section

Materials. CeO_2 and TiO_2 (99.9%, Sigma Aldrich) were used as the lanthanide and titanium sources while V_2O_5 (S. D. Fine Chem. 99%) was the source for vanadium. Methylene blue (MB), Remazol brilliant blue (RBBR), Orange G (OG), Malachite Green (MG), Rhodamine B (RB), Alizarine S (ARS), Rhodamine Blue (RBL), phenol (PH), 4-chlorophenol (4CLPH), 2-chlorophenol (2CLPH), 2-nitrophenol (2NPH), 4-nitrophenol (4NPH), 2,4-dichlorophenol (DCP), 2,4-dinitrophenol (DNP), 2-nitro-4-chlorophenol, and 4-nitro-2-chlorophenol (all from S. D. Fine Chem Ltd., India) were used as supplied without

* To whom correspondence should be addressed. Tel: +91-80-2292796. Fax: +91-80-3601310. E-mail: ssctng@sscu.iisc.ernet.in.
[†] Solid State and Structural Chemistry Unit.
[‡] Department of Chemical Engineering.

10.1021/ie9006134 CCC: $40.75
Published on Web 07/15/2009

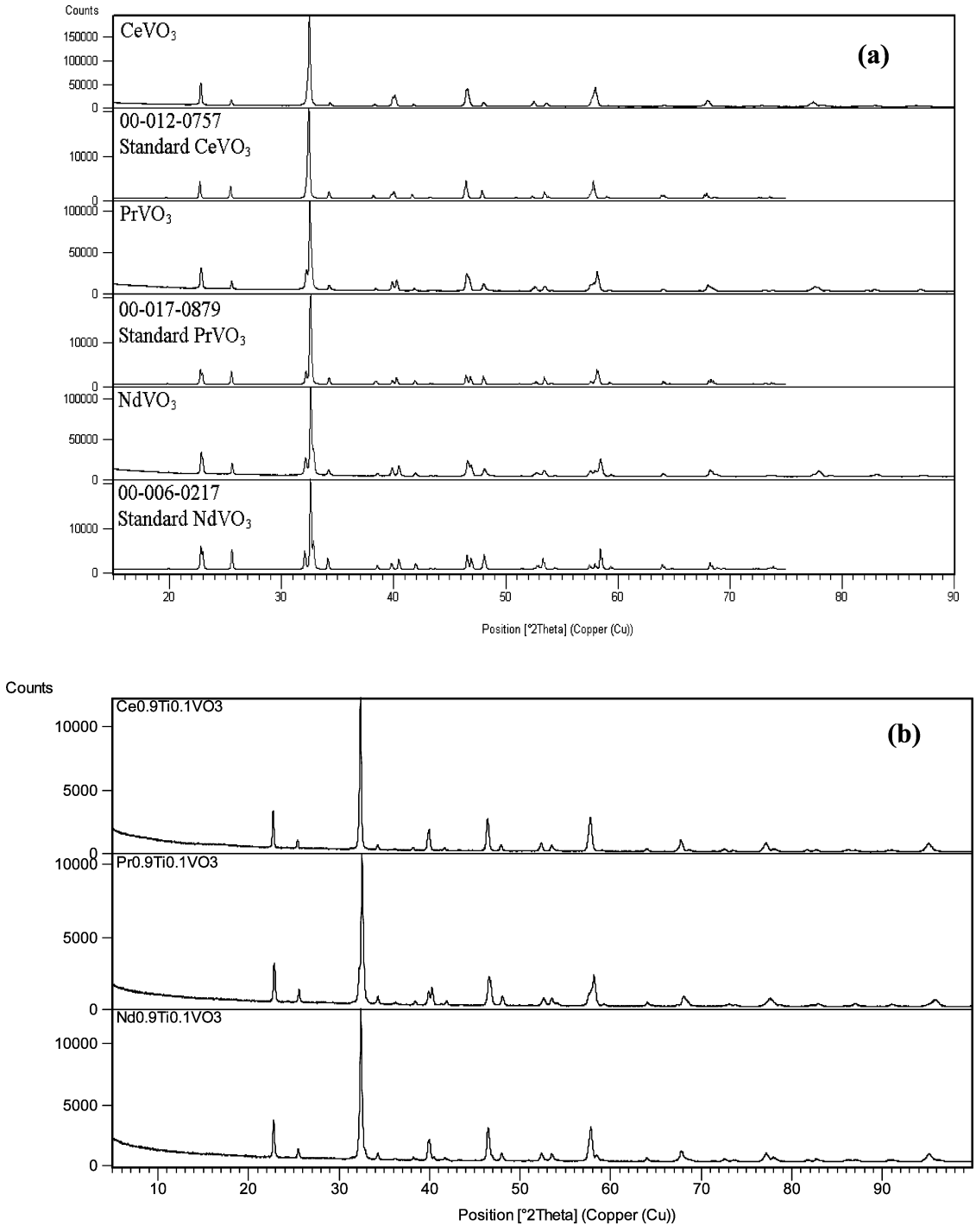

Figure 1. Powder X-ray diffraction pattern of synthesized (a) $LnVO_3$ and (b) $Ln_{0.9}Ti_{0.1}VO_3$ (Ln = Ce, Pr and Nd).

further purification. Water was distilled twice and filtered through a Millipore membrane before use.

Preparation. $LnVO_3$ (Ln = Ce, Pr, Nd) and Ti substituted $LnVO_3$ were synthesized by a solid state method using lanthanide oxides CeO_2, Pr_6O_{11}, and Nd_2O_3, respectively, and V_2O_5 in stoichiometric quantities. For $LnVO_3$ stoichiometric amounts of starting materials were ground in an agate mortar and made into pellets. The pellets were fired at 700 °C with a heating rate of 20 °C/min and held for 6 h followed by an increase to 800 °C at a heating rate of 20 °C/min and again held for 6 h. This treatment gave rise to precursor $LnVO_4$ (Ln = Ce, Pr, Nd), where Ln, V, and O are in +3, +5, and −2 oxidation state. The precursors were finally reduced at 900 °C under flowing H_2 for 24 h to obtain the desired product $Ln^{3+}V^{+3}O_3$ (Figure 1a). However, for $Ln_{0.9}Ti_{0.1}VO_3$ stoichiometric amounts of starting materials were ground in an agate mortar, made into pellets, and heated to 900 °C under flowing H_2 for 24 h resulting in the desired product, $Ln^{3+}{}_{0.1}T^{+4}i_{0.9}V^{+3}O_3$ (Figure 1b).

Characterization. Morphology and composition analysis of $LnVO_3$ (Ln = Ce, Pr, and Nd) samples were carried out with the help of FEI Quanta scanning electron microscope (Figure S1, see Supporting Information). UV−vis absorption spectra (Figure S2a,b, see Supporting Information) of $LnVO_3$ and $Ln_{0.9}Ti_{0.1}VO_3$ (Ln = Ce, Pr, and Nd) show a broad absorption band starting from 800 to 200 nm. The compositional and oxidation state analyses were performed with X-ray photoelectron spectroscopic (XPS) measurement on a VG MicroTech ESCA 3000 instrument at a pressure of $>1 \times 10^{-9}$ Torr (pass

energy of 50 eV, electron takeoff angle 60°, and overall resolution ~1 eV).

Surface Area Analysis. BET analysis of all the samples was carried out using a porosimeter (Belsorp, Japan). The surface areas of all the materials were less than 1 m^2/g.

X-ray Powder Diffraction. X-ray diffraction data for the samples were collected on a D8 Advance Bruker and Philips X'pert pro powder diffractometer in the range 2θ from 5 to 90° with a step size of 0.008° and 5 s exposure time/step.

Photochemical Reactor. The photochemical reactor used in this study was made of a jacketed quartz tube of 3.4 cm internal diameter, 4 cm outer diameter, and 21 cm length and an outer Pyrex glass reactor of 5.7 cm internal diameter and 16 cm length. A high pressure mercury vapor lamp (HPML) of 125 W (Philips, India) was placed inside the jacketed quartz tube after the removal of the outer shell. To avoid the fluctuations in the input, supply ballast and capacitor were connected in series with the lamp. Water was circulated through the annulus of the quartz tube to avoid heating of the solution. A total of 100 mL of the solution was taken in the outer reactor and continuously stirred to ensure that the suspension of the catalyst was uniform. The lamp radiated predominantly at 365 nm corresponding to the energy of 3.4 eV and photon flux of 5.8×10^{-6} mol of photons/s. Further details of the experimental setup has been described elsewhere.[28]

Degradation Experiments. Aqueous solutions of all dyes and organic compounds were taken in the reactor with a catalyst loading of 1 g/L. The mixture was stirred for 12 h in dark and the resulting concentration was taken as initial concentration after adsorption. The reactions were carried out at ~40 °C, which was maintained by circulating water in the annulus of the jacketed quartz reactor. No adjustment of pH was done during the experiment. The degradation experiment was carried out for 1 h during which samples were collected at the regular interval of time. The collected samples were then filtered and centrifuged for about an hour to remove any catalyst particles before the analysis.

Sample Analysis. All dyes were analyzed with a UV−visible spectrometer (Lambda 32 Perkin-Elmer). The calibration for MB, RBBR, OG, ARS, MG, RB, and RBL was based on the Beer−Lambert law at their maximum absorption wavelength, λ_{max}, of 665, 591, 489, 424, 617, 554, and 664 nm, respectively. All the organic compounds were analyzed by HPLC (Waters Inc.) with a C18 reverse phase column. During the analysis 10% methanol was taken as the eluent with a flow rate of 0.5 mL/min. The calibration for phenol, 4-chlorophenol, 2-chlorophenol, 2-nitrophenol, 4-nitrophenol, 2,4-dinitrophenol, 2,4-dichlorophenol, 2-nitro-4-chlorophenol, and 4-nitro-2-chlorophenol was based on the Beer−Lambert law at its maximum absorption wavelength, λ_{max}, of 270, 275, 280, 280, 320, 280, 292, 270, and 320 nm, respectively.

Results and Discussion

Crystal Structure. Powder diffraction data show the formation of single phase orthorhombic perovskite type $LnVO_3$ compounds. The diffraction patterns for $CeVO_3$, $PrVO_3$, and $NdVO_3$ match with the JCPDS database nos. 00-012-0757, 00-017-0879, and 00-006-0217, respectively (Figure 1a). Rietveld refinements were carried out using GSAS[29] for each X-ray powder diffraction pattern in the space group *Pnma*. During the refinement full occupancy was assigned to each atom with known coordinates and cell parameters taken from the reported literature data.[30] Wyckoff sites, 8*d*, 4*c*, 4*c*, and 4*b*, were assigned for O1, Ln (Ce, Pr, and Nd), O2, and V, respectively. All synthesized $LnVO_3$ have orthorhombic perovskite type structure in which Ln^{3+} is eight coordinated with two different kinds of oxygen, O1 and O2. It is clear from the bond distances and bond angles that the edge and corner sharing polyhedra of LnO_8 is distorted (see the Supporting Information, Figure S3). The V^{3+} is octahedrally coordinated with both types of oxygen atoms. Both the LnO_8 and VO_6 polyhedra share faces with each other, while VO_6 octahedra in the structure are tilted with oxygen atoms sharing the corner as shown in (see the Supporting Information, Figure S3). The observed and calculated profiles resulting from GSAS runs for $CeVO_3$, hereafter, taken as a representative member of $LnVO_3$, are shown in Figure 2. Crystallographic refined parameters, atomic coordinates, isotropic temperature factors, and occupancy for $CeVO_3$ are listed in Table 1. Bond lengths and bond angles are listed in Tables S1 and S2 (see Supporting Information), respectively.

A single phase solid solution of $Ce_{0.9}Ti_{0.1}VO_3$ was obtained, and the powder pattern matches with that of the parent compound $LnVO_3$. It was initially assumed that Ti would get reduced (Ti^{2+} ionic radius = 0.86 or Ti^{3+} ionic radius = 0.67) under hydrogen atmosphere and partially occupy the Ln position. This situation is similar to Pt^{2+} substitution at the A site in the structure of $LaMnO_3$ and Li^{1+} substitution at the A site in $LaTiO_3$ (Pt^{2+} ionic radius = 0.8 and Li^{1+} ionic radius = 0.92, respectively).[31,32] On the basis of the literature of ABO_3 compounds, the A site can be partially replaced by elements with +1, +2, and +3 oxidation states.[7] The XPS studies on the representative sample, $Ce_{0.9}Ti_{0.1}VO_3$, showed that Ti is in the +4 oxidation state (see Supporting Information, Figure S4a). Further, the oxidation state of vanadium is indicated to be either +3 (ionic radii = 0.64) or +5 (ionic radii = 0.54) (see the Supporting Information, Figure S4b), and hence its partial presence at the A site can be anticipated. A new probable chemical formula $[Ce_{0.9}V_{0.1}][Ti_{0.1}V_{0.9}]O_3$ was proposed on the basis of these observations. This composition suggests an incorporation of 10% Ti at the vanadium site with the excess vanadium shifting to the A site with an oxidation state of +3.

To unequivocally establish the composition of these compounds, difference Fourier methodology was adopted. Fourier synthesis provides a useful tool to arrive at the proper composition. These studies were carried out using GSAS[29] wherein the occupancy of each site was monitored. The observed and calculated profile of $[Ce_{0.9}V_{0.1}][Ti_{0.1}V_{0.9}]O_3$ is shown in Figure 3. The scattering factors associated with the Ce atom are substantially higher than those associated with Ti and V atoms. Since Ti and V are neighbors in the periodic table, the effective occupancy analysis needs to be done with care. The evidence provided by XPS analysis clearly suggests the absence of Ti in the A site. Figure 4a shows the difference Fourier map for the parent compound $CeVO_3$. The residual electron density is essentially concentrated in the bonding region, and both A and B sites show negligible density accumulation. Figure 4b is for the composition $[Ce_{0.9}V_{0.1}][Ti_{0.1}V_{0.9}]O_3$, and the residual density is mainly restricted to the bonding region. To evaluate the correctness of this assignment, occupancies of A and B sites were altered, and the corresponding difference Fourier analyses are shown in Figure 4c,d. Significant residual electron density accumulation is observed in each of these cases at either A or B sites. Figure 4c represents the composition $[Ce_1][Ti_{0.1}V_{0.9}]O_3$. There is an accumulation of electron density at the V site. This feature can be interpreted as follows. The stoichiometry implies 10% less V in the structure, and the Ce site has excess electron density (10% more Ce) than required. Ce being a much heavier element, the scattering power is significantly larger at higher

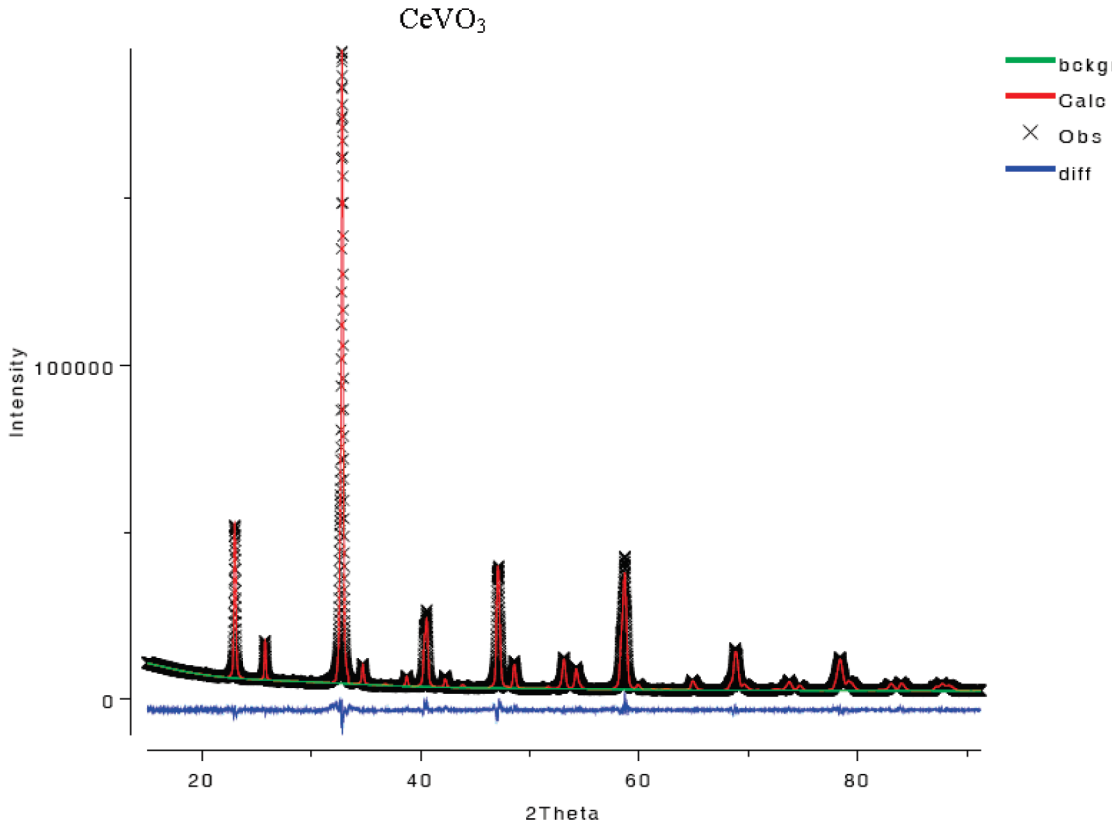

Figure 2. Calculated (red) and observed (black) profile for $CeVO_3$.

Table 1. Crystallographic Refined Parameters

parameter	$CeVO_3$	$Ce_{0.9}T_{0.1}VO_3$
λ (Å)	1.5418	1.5418
crystal system	orthorhombic	orthorhombic
space group	*Pnma*	*Pnma*
a **(Å)**	5.494(2)	5.549(1)
b **(Å)**	7.717(4)	7.802(1)
c **(Å)**	5.453(4)	5.516(1)
V **(Å^3)**	231.163(1)	238.854(1)
ρ_{calc} (g cm^{-3})	6.869	6.391
R_p	0.0320	0.0425
R_{wp}	0.0451	0.0495
DWd	0.195	0.787
CHI2**	11.84	1.385

$CeVO_3$

	Ce	V	O1	O2
x	0.463(1)	0	0.206(1)	0.509(1)
y	0.25	0	0.025	0.25
z	0.008(1)	0	0.286(1)	0.594(1)
k	1	1	1	1
B	0.002(1)	0.003(1)	0.007(1)	0.019(1)

$Ce_{0.9}T_{0.1}VO_3$

	Ce	Vi	Ti	V2	O1	O2
x	0.464(1)	0.464(1)	0	0	0.215(1)	0.009(1)
y	0.25	0.25	0	0	0.034(1)	0.25
z	0.002(1)	0.002(1)	0	0	0.291(1)	0.903(1)
k	0.9	0.1	0.1	0.9	1	1
B	0.002(1)	0.002(1)	0.005(1)	0.005(1)	0.005(1)	0.005(1)

sin θ/λ values than those of vanadium and titanium. The lack of vanadium occupancy along with the excess occupancy at the Ce site causes the appearance of excess electron density at the vanadium site (Figure 4c). To further rationalize these observations, the composition was changed to $[Ce_{0.5}V_{0.5}][Ti_{0.5}V_{0.5}]O_3$, and Figure 4d indicates an anticipated electron density excess at the Ce site. Hence, it may be concluded that the correct composition is $[Ce_{0.9}V_{0.1}][Ti_{0.1}V_{0.9}]O_3$. This exercise demonstrates the power of difference Fourier analysis in such cases where the extent of substitution is around 10%.

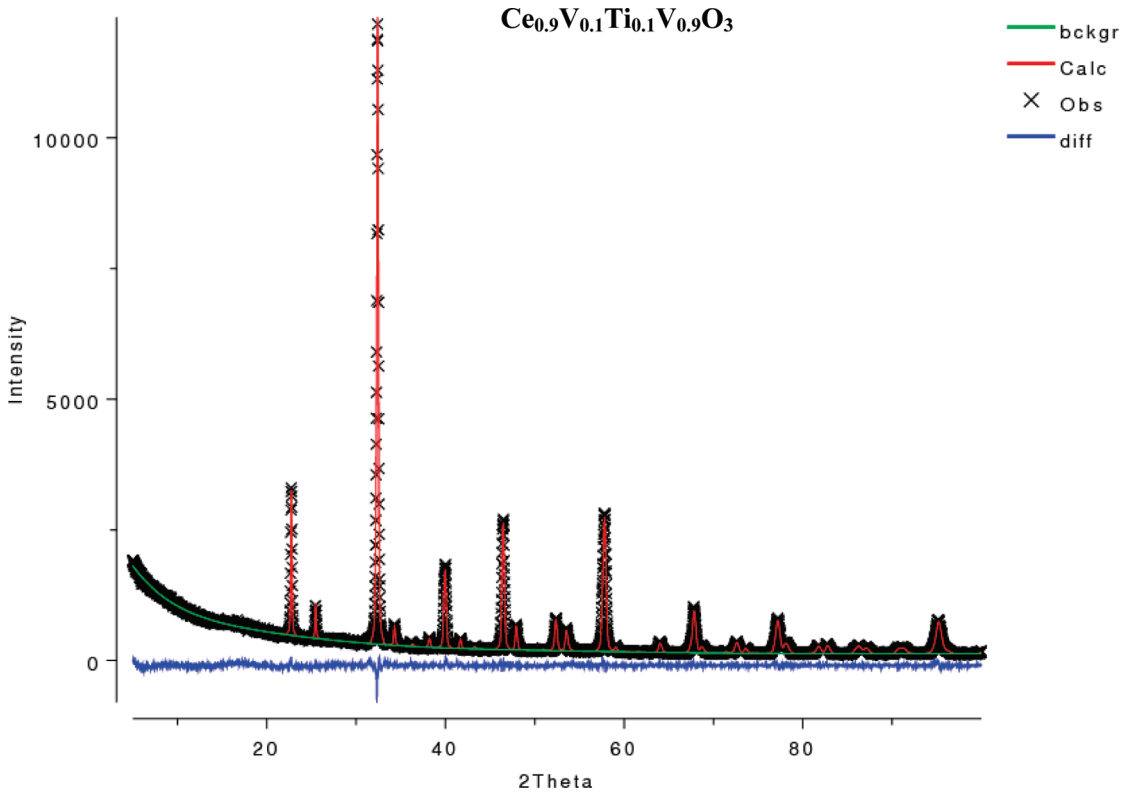

Figure 3. Calculated (red) and observed (black) profile for $[Ce_{0.9}V_{0.1}][Ti_{0.1}V_{0.9}]O_3$.

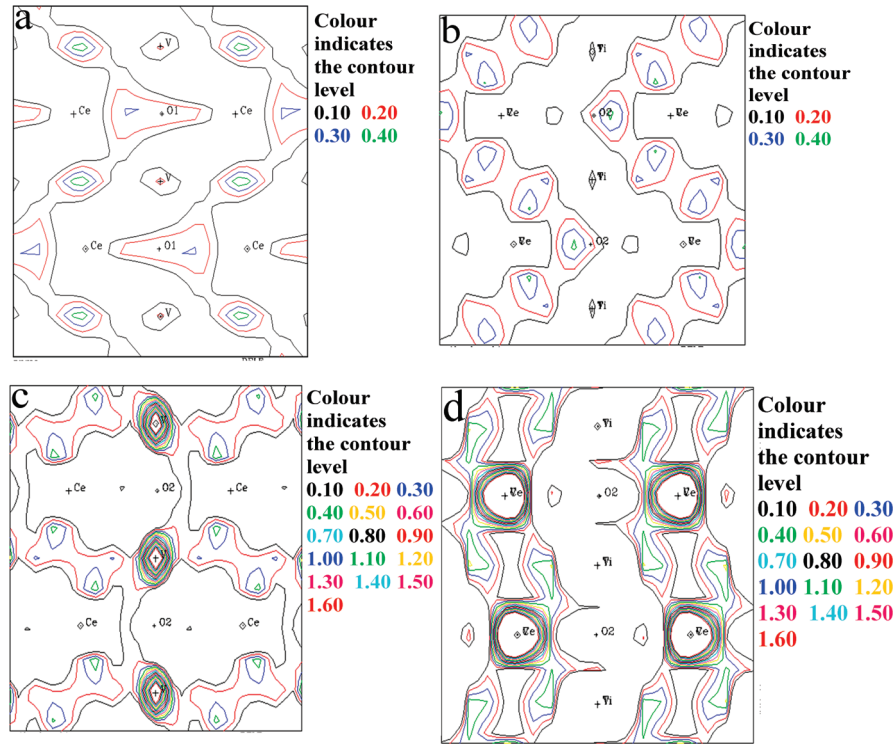

Figure 4. Difference Fourier map of (a) $CeVO_3$, (b) $Ce_{0.9}V_{0.1}Ti_{0.1}V_{0.1}O_3$, (c) $[Ce_1][Ti_{0.1}V_{0.9}]O_3$, and (d) $[Ce_{0.5}V_{0.5}][Ti_{0.5}V_{0.5}]O_3$.

Photocatalysis. Photocatalytic degradation of different dyes and organics was carried out in the presence of $LnVO_3$ and $Ln_{0.9}Ti_{0.1}VO_3$ (Ln = Ce, Pr, and Nd) catalysts. The unsubstituted $LnVO_3$ compounds show catalytic activity toward cationic chlorinated xanthane dyes like RBL (Figure 5). However, the catalytic activity for the degradation of anionic sulfonated azo dye (OG) and sulfonated anthroquinonic dye (RBBR) and heteropolyaromatic cationic dye (MB), cationic dye Malachite Green (MG), and nonchlorinated cationic Xanthane Dye (RB) was negligible (Figure 5 and Figure S5a,b, see Supporting Information). So it appears that $LnVO_3$ compounds are specific to chlorinated dyes. To verify chlorospecificity for the degradation of organics by $LnVO_3$, photocatalytic degradation experiments of various organics like phenol, 4-chlorophenol, and 2,4-dichlorophenol were carried out. It was found that after one hour of degradation, the concentration of phenol was not reduced

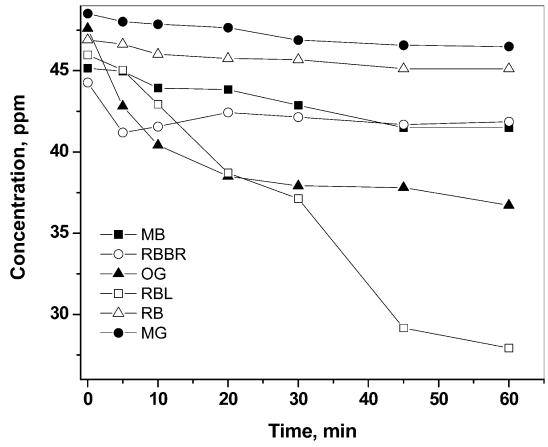

Figure 5. Degradation profiles of all dyes in presence of $CeVO_3$.

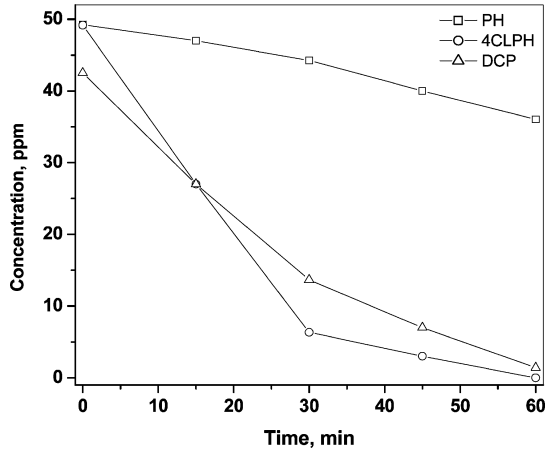

Figure 6. Degradation profiles of phenol, dichlorophenol, and 4-chlorophenol in presence of $CeVO_3$.

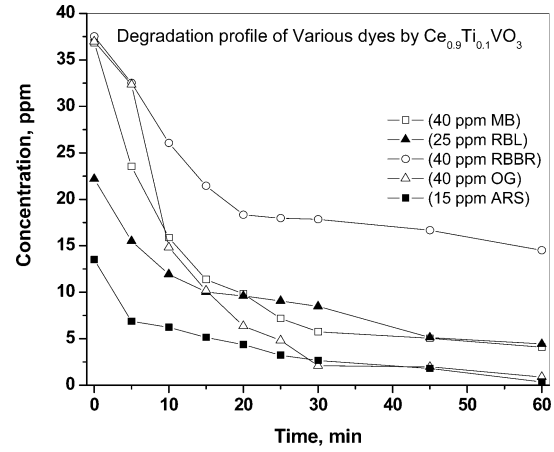

Figure 7. Degradation profiles of various dyes in presence of $Ce_{0.9}Ti_{0.1}VO_3$.

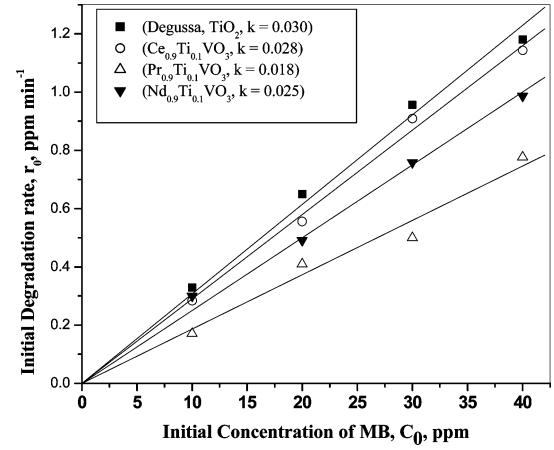

Figure 8. Variation of the initial rate with initial concentration for the degradation of methylene blue in presence of Degussa TiO_2, $Ce_{0.9}Ti_{0.1}VO_3$, $Pr_{0.9}Ti_{0.1}VO_3$, and $Nd_{0.9}Ti_{0.1}VO_3$.

while the concentrations of 2,4-dichlorophenol and 4-chlorophenol were reduced from 50 ppm to less than 1 ppm (Figure 6 and Supporting Information, Figure S6a,b). This confirms that $LnVO_3$ selectively degrades chloro-substituted phenols.

Titanium substituted $LnVO_3$ also shows similar UV diffuse reflectance spectra, which indicates that these compounds can also be used as photocatalysts. Various classes of cationic dyes like heteropolyaromatic (MB) and Xanthane (RBL) and three anionic dyes like sulfonated azoic (OG) and sulfonated anthroquinonic (RBBR and ARS) were considered. As discussed earlier, $LnVO_3$ preferentially degrades chloro-substituted compounds only. However, Ti substituted $LnVO_3$ degraded all classes of dyes. The degradation profiles for MB, RBL, OG, RBBR, and ARS in the presence of $Ce_{0.9}Ti_{0.1}VO_3$ are given in Figure 7. The initial rate (r_0) for the degradation of the dye was calculated from the change in the concentration, that is, from $(C_0 - C_t)/t$, where C_0 is initial concentration of the dye and C_t is the concentration of the dye at time t. To calculate the initial rate, t was taken as 30 min. The initial rate was calculated for various initial dye concentrations. The rate constant k was calculated by plotting the variation of the initial rate with initial concentrations (Figure 8). The degradation was compared with commercial Degussa P-25 TiO_2 (Figure S7a−d). The overall kinetic rate constants (k) for the degradation of methylene blue in presence of Degussa P-25 and $Ln_{0.9}Ti_{0.1}VO_3$ (Ce, Pr, and Nd) are found to be 0.03, 0.028, 0.018, and 0.025 min^{-1}, respectively. A comparative degradation profile of RBL, OG, RBBR, and ARS dyes by Degussa P-25, $Ce_{0.9}Ti_{0.1}VO_3$, $Pr_{0.9}Ti_{0.1}VO_3$, and $Nd_{0.9}Ti_{0.1}VO_3$ is given in Figure S8a−d (see Supporting Information), respectively. All the catalysts degrade both anionic and cationic dyes at nearly the same rates.

To verify whether the chlorospecificity in the Ti substituted compounds, phenol and chloro- and nitro-substituted phenol were tested for degradation. Figure 9a shows that the concentration of phenol decreased from 50 ppm to 25 ppm in the presence of Degussa P-25 and $Pr_{0.9}Ti_{0.1}VO_3$. However, the degradation was negligible in the presence of $Ce_{0.9}Ti_{0.1}VO_3$ and $Nd_{0.9}Ti_{0.1}VO_3$. The substitution of chlorine was examined by degrading 2,4-dichlorophenol (DCP) in the presence of all the compounds (Figure 9b). The degradation rate of DCP was significant and followed the order Degussa P-25 $\approx$ $Pr_{0.9}Ti_{0.1}VO_3$ > $Ce_{0.9}Ti_{0.1}VO_3$ > $Nd_{0.9}Ti_{0.1}VO_3$. This indicates among all the investigated $Ln_{0.9}Ti_{0.1}VO_3$ that $Pr_{0.9}Ti_{0.1}VO_3$ is the most active in degrading chloro containing organics. Further, to verify the chlorospecificity of $Pr_{0.9}Ti_{0.1}VO_3$, 2-chloro, 4-chloro, 2-chloro-4-nitro, and 4-chloro-2-nitro phenol were taken for degradation (Figure 10). The degradation profile shows the following trend 4-chloro > 2-chloro > 4-chloro-2nitro > 2-chloro-4-nitro, indictating that 4-chloro organics degrade faster in the presence of $Pr_{0.9}Ti_{0.1}VO_3$.

Our previous studies[33–35] indicated that nitro compounds can be specifically degraded. To examine the nitro specificity, we followed a similar procedure as above. The degradation profile of 2,4-dinitrophenol (DNP) in the presence of all Ti substituted $LnVO_3$ (Figure 11) follows the order Degussa P-25 $\approx$ $Nd_{0.9}Ti_{0.1}VO_3$ > $Ce_{0.9}Ti_{0.1}VO_3$ $\approx$ $Pr_{0.9}Ti_{0.1}VO_3$. The above

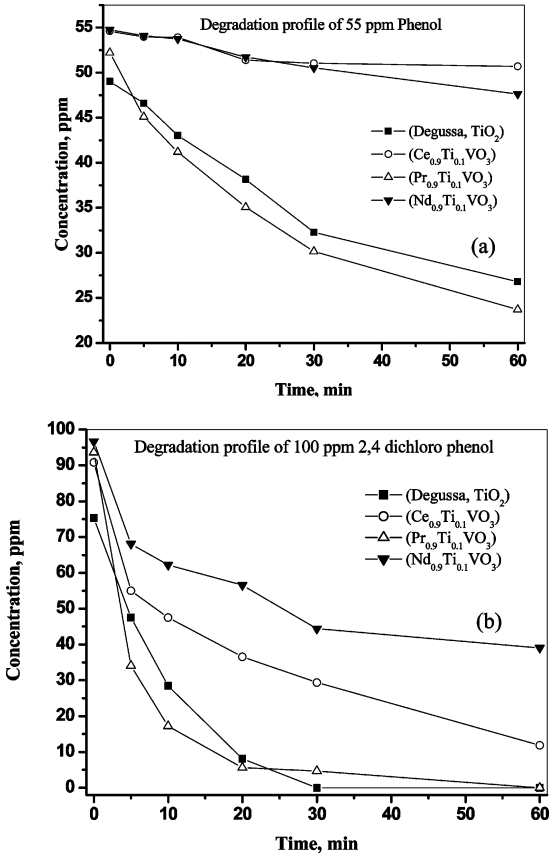

Figure 9. Degradation profiles of (a) phenol and (b) 2,4-dichlorophenol in presence of Degussa- TiO_2, $Ce_{0.9}Ti_{0.1}VO_3$, $Pr_{0.9}Ti_{0.1}VO_3$, and $Nd_{0.9}Ti_{0.1}VO_3$.

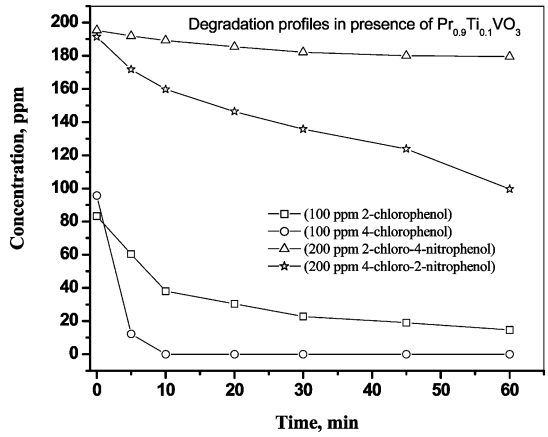

Figure 10. Degradation profiles of chlorosubstituted phenol in presence of $Pr_{0.9}Ti_{0.1}VO_3$.

observation indicates that among the various $Ln_{0.9}Ti_{0.1}VO_3$ investigated in this study, $Nd_{0.9}Ti_{0.1}VO_3$ is the most active for the photodegradation of nitro-substituted phenols. To check nitrospecificity of $Nd_{0.9}Ti_{0.1}VO_3$, 2-nitro, 4-nitro, 2-chloro-4-nitro, and 4-chloro-2-nitro phenol were taken for degradation (Figure 12). The degradation profile shows a negligible decrease in concentration in the case of 4-nitro and 2-chloro-4-nitrophenol, whereas there is considerable degradation in the case of 2-nitro and 4-chloro-2-nitro phenol. This observation clearly indicates $Nd_{0.9}Ti_{0.1}VO_3$ degrades 2-nitro containing organics in preference to 4-nitro containing organics.

From the above experiment it can be concluded that the internal structure of the compound plays a more important role

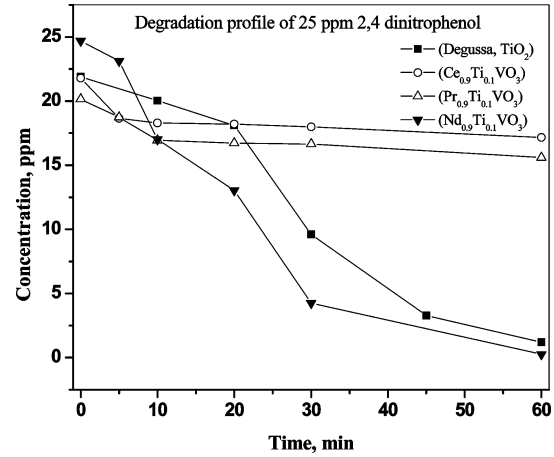

Figure 11. Degradation profiles of 2,4-dinitrophenol (DNP) in the presence of $Ln_{0.9}Ti_{0.1}VO_3$ (Ln = Ce, Pr, Nd).

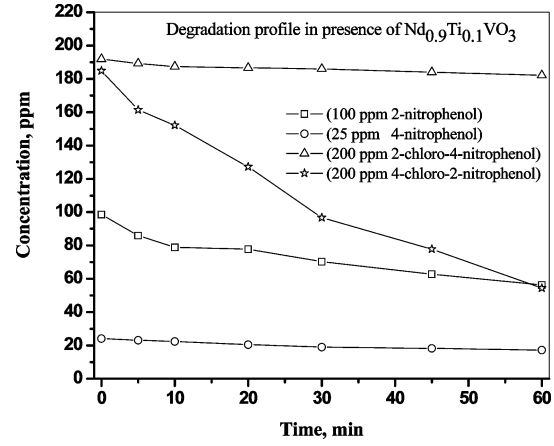

Figure 12. Degradation profile of nitrosubstituted phenol in the presence of $Nd_{0.9}Ti_{0.1}VO_3$.

than the surface area for the photodegradation. In the current case, even though the surface area is less than 1 m^2/g the catalytic effect is comparable to that for commercial catalyst Degussa P-25, which has a surface area of 50 m^2/g. The reason for photocatalytic activity may be attributed to the broad UV reflectance band over a wide range. This study is consistent with a previous study that investigated $CaIn_2O_4$ and showed that, despite very low surface area (<1 m^2/g), the material showed very high photocatalytic activity due to the presence of regular InO_6 octahedra. Tang et al.[36] investigated a series of MIn_2O_4 (M = Ca, Sr, Ba) photocatalysts and showed that the Ca substituted material showed the highest photocatalytic activity, although its light absorption ability was the lowest. This was attributed to the excellent photoelectron transfer ability of $CaIn_2O_4$ due to the distorted octahedra structure. It was also reported that the materials composed of the uniform InO_6 octahedra network are beneficial to the charge transfer to the surface of the materials.[36,37]

Similarly the presence of VO_6 octahedra in $LnVO_3$ and $Ln_{0.9}Ti_{0.1}VO_3$ may be responsible for photocatalytic activity. Orthorhombic perovskite type $Ln^{3+}V^{+3}O_3$ and orthovanadate $Ln^{3+}V^{+5}O_4$ have regular polyhedra of VO_6 and VO_4, respectively. In our previous study,[35] we have found that $LnVO_4$ compounds exhibit photocatalytic activity comparable to the commercial catalyst Degussa P-25. The XPS analysis of $LnVO_3$ indicates that the majority of vanadium is in the +3 oxidation state, whereas it is in the +5 state in the case of $LnVO_4$. Despite the presence of the regular polyhedra in both the cases, it is not

possible to compare the photocatalytic activity of the compounds because the structural motif is different in both cases.

It might be suggested that the formation of a bond between chlorophenols and vanadium is responsible for the chlorospecificty which is similar to the chlorospecificity that was observed in $BaBi_2Mo_{4-x}W_xO_{16}$ where the bond formation is between Mo and chlorophenol.[38,39] The partial doping of Ti to at the vanadium site and the subsequent shifting of 10% V to the Ln site might create vacancies at the cation site resulting in a possible increase in photo-activity. This is consistent with previous studies[38] that show that the presence of vacancies at the cation site leads to superior photocatalytic activity.

Conclusions

A comparative photocatalytic study of $LnVO_3$ (Ln = Ce, Pr and Nd), and its titanium substituted compounds ($Ln_{0.9}Ti_{0.1}VO_3$) has been investigated. The composition for the Ti substituted lanthanum vanadate was determined by difference Fourier methodology to be $[Ln_{0.9}V_{0.1}][Ti_{0.1}V_{0.9}]O_3$. The Ti substituted compounds were found to be more active compared to their unsubstituted parent compounds for the photocatalytic degradation of dyes and organics. $Pr_{0.9}Ti_{0.1}VO_3$ degrades 4-chloro containing phenol preferentially, whereas $Nd_{0.9}Ti_{0.1}VO_3$ predominantly degrades 2-nitro containing organics. The higher catalytic activity in the Ti substituted compound is due to the presence of VO_6 octahedra which is beneficial for availability of surface electrons, and the incorporation of the titanium to the vanadium site leads to cation vacancy which further assists photocatalytic behavior.

Acknowledgment

We acknowledge funding from DST, India, and acknowledge financial support for the XRD machine under the DST-FIST program. S.M. thanks CSIR India for providing a research associateship. The authors thank Mr. I. S. Jarali for surface area analysis and B.R. Sathe, NCL, Pune, India, for XPS analysis.

Supporting Information Available: Bond distances and selected bond angles of $CeVO_3$ and $Ce_{0.9}Ti_{0.1}VO_3$ (Tables S1 and S2); SEM image of $LnVO_3$ (Figure S1); UV diffuse reflectance of $LnVO_3$ and $Ln_{0.9}Ti_{0.1}VO_3$ (Figure S2a,b); a representative orthorhombic perovskite type structure of $LnVO_3$ showing LnO_8 polyhedra and VO_6 octahedra (Figure S3); XPS analysis of $Ce_{0.9}Ti_{0.1}VO_3$ showing (a) Ti^{4+} and (b) V^{3+} and V^{5+} oxidation states (Figure S4); various degradation profiles of various dyes in the presence of (a) $PrVO_3$ and (b) $NdVO_3$ (Figure S5); degradation profile of chlorosubstituted phenols in the presence of (a) $PrVO_3$ and (b) $NdVO_3$ (Figure S6); degradation profile of (a) 10, (b) 20, (c) 30, and (d) 40 ppm MB in the presence of Degussa TiO_2 and $Ln_{0.9}Ti_{0.1}VO_3$ (Ln = Ce, Pr, and Nd) (Figure S7); and degradation profiles of (a) RBL, (b) OG, (c) RBBR and (d) ARS in presence of Degussa TiO_2 and $Ln_{0.9}Ti_{0.1}VO_3$ (Ln = Ce, Pr and Nd) (Figure S8). This material is available free of charge via the Internet at http://pubs.acs.org.

Literature Cited

(1) *Catalytic Chemistry of Solid State Inorganics*, Moser, W. R., Ed.; New York Academy of Sciences: New York, 1976.

(2) Centi, G.; Trifiro, F. Oxidation Catalysts Based on Antimony Mixed Oxides with Rutile-type Structures. *Catal. Rev.-Sci. Eng.* **1986**, *28*, 165.

(3) Mizuno, N.; Misono, M. Heterogeneous Catalysis. *Chem. Rev.* **1998**, *98*, 199.

(4) *Properties and Applications of Perovskite Type Oxides*; Tejuca, L. J., Fierro, J. L. G., Eds.; Marcel Dekker: New York, 1993.

(5) Raveau, B. In *Proceedings of the Indian National Science Academy Symposium Solid State Chemistry*; Rao, C. N. R., Ed.; Indian National Science Academy: New Delhi, 1986; Part A, Vol. 52, p 67.

(6) Bednorz, J. G.; Muller, K. A. Perovskite-Type Oxides - the New Approach to High-T Superconductivity. *Angew. Chem., Int. Ed. Engl.* **1988**, *100*, 735.

(7) Pena, M. A.; Fierro, J. L. G. Chemical Structures and Performance of Perovskite Oxides. *Chem. Rev.* **2001**, *101*, 1981.

(8) Sayagues, M. J.; Vallet-Regí, M.; Caneiro, A.; Gonzalez-Calbet, J. M. Microstructural Characterization of the $LaNiO_{3-y}$ System. *J. Solid State Chem.* **1994**, *110*, 295.

(9) Smyth, D. M. In *Properties and Applications of Perovskite-Type Oxides*, Tejuca, L. G., Fierro, J. L. G., Eds.; Marcel Dekker: NewYork, 1993; p 47.

(10) Bringley, J. F.; Scott, B. A.; La Placa, S. J.; Boehme, R. F.; Shaw, T. M.; McElfresh, M. W.; Trail, S. S.; Cox, D. E. Synthesis of the Defect Perovskite Series $LaCu0_{3-\delta}$ with Copper Valence Varying from 2+ to 3+. *Nature* **1990**, *347*, 263.

(11) Tofield, B. C.; Scott, W. R. Oxidative Nonstoichiometry in Perovskites, an Experimental Survey; the Defect Structure of an Oxidized Lanthanum Manganite by Powder Neutron Diffraction. *J. Solid State Chem.* **1974**, *10*, 183.

(12) Han, Y. H.; Harmer, M. P.; Hu, Y. H.; Smyth, D. M. In *Transport in Non-stoichiometric Compounds*, Simkovich, G., Stubican, V. S., Eds.; Plenum: New York, 1985; p 73.

(13) Yan, J. Q.; Zhou, J. S.; Goodenough, J. B. Unusually Strong Orbit-Lattice Interactions in the RVO_3 Perovskites. *Phys. Rev. Lett.* **2004**, *93*, 2359011.

(14) Ren, Y.; Nugroho, A. A.; Menovsky, A. A.; Strmpfer, J.; Rütt, U.; Iga, F.; Takabatake, T.; Kimball, C. W. Orbital-ordering-induced Phase Transition in $LaVO_3$ and $CeVO_3$. *Phys. Rev. B* **2003**, *67*, 0141071.

(15) Wang, F.; Zhang, J.; Yuan, P.; Yan, Q.; Zhang, P. Magnetic and transport properties of vanadate $PrVO_3$. *J. Phys.: Condens. Matter* **2000**, *12*, 3037.

(16) Kimishima, Y.; Takahashi, M.; Iga, K.; Ishikawa, H.; Okada, K.; Ichiyanagi, Y. Paramagnetism in $SmVO_3$ and $EuVO_3$. *Physica B* **1994**, *211*, 194.

(17) Kimishima, Y.; Ichiyanagi, Y.; Shimizu, K.; Mizuno, T. N-type Ferrimagnetism of $SmVO_3$. *J. Magn. Magn. Mater.* **2000**, *210*, 244.

(18) Kimishima, Y.; Nishida, S.; Mizuno, T.; Ichiyanagi, Y.; Uehara, M. Pressure Effects on N-type Ferrimagnet $SmVO_3$. *Solid State Commun.* **2002**, *122*, 519.

(19) Kimishima, Y.; Uehara, M.; Saitoh, T. Ca-doping effects on N-type ferrimagnetism of $NdVO_3$. *Solid State Commun.* **2005**, *133*, 559.

(20) Li, Y.; Qin, S.; Seifert, F. Substitution in *A*-site substituted perovskite compounds: The $Ca_{1-2x}Na_xLa_xTiO_3$ ($0 \le x \le 0.5$) solid solution. *J. Solid State Chem.* **2007**, *180*, 824.

(21) Hoffmann, M. R.; Martin, S. T.; Choi, W.; Bahnemann, D. W. Environmental Applications of Semiconductor Photocatalysis. *Chem. Rev.* **1995**, *95*, 69.

(22) Stafford, U.; Gray, K. A.; Kamat, P. V. Photocatalytic Degradation of Organic Contaminants. Halophenols and Related Model Compounds. *Heterog. Chem. Rev.* **1996**, *3*, 77.

(23) Wrighton, M. S.; Ellis, A. B.; Wolczanski, P. T.; Morse, D. L.; Abrahamson, H. B.; Ginley, D. S. Strontium Titanate Photoelectrodes. Efficient Photoassisted Electrolysis of Water at Zero Applied Potential. *J. Am. Chem. Soc.* **1976**, *98*, 2774.

(24) Mitsui, C.; Nishiguchi, H.; Fukamachi, K.; Ishihara, T.; Takita, Y. Photocatalytic Decomposition of Pure Water over NiO Supported on $KTa(M)O_3$ ($M = Ti^{4+}$, Hf^{4+}, Zr^{4+}) Perovskite Oxide. *Chem. Lett.* **1999**, 1327.

(25) Sato, S.; Kadowaki, T. Photocatalytic Activities of Metal Oxide Semiconductors for Oxygen Isotope Exchange and Oxidation Reactions. *J. Catal.* **1987**, *106*, 295.

(26) Van Damme, H.; Hall, W. K. Photocatalytic Properties of Perovskites for H_2 and CO Oxidation—Influence of Ferroelectric Properties. *J. Catal.* **1981**, *69*, 371.

(27) Miyama, H.; Fujii, N.; Nagac, Y. Heterogeneous Photocatalytic Synthesis of Ammonia from Water and Nitrogen. *Chem. Phys. Lett.* **1980**, *74*, 523.

(28) Sivalingam, G.; Nagaveni, K.; Hegde, M. S.; Madras, G. Photocatalytic Degradation of Various Dyes by Combustion Synthesized Nano Anatase TiO_2. *Appl. Catal., B* **2003**, *45*, 23.

(29) Larson, A. C.; Von Dreele, R. B. *General Structure Analysis System (GSAS)*; Los Alamos National Laboratory Report, LAUR 86-748, Los Alamos National Laboratory: Los Alamos, NM, 2004.

(30) Yoshii, K.; Abe, H. Magnetic Properties of $LnTi_{0.5}V_{0.5}O_3$ (Ln = Ce and Pr). *J. Solid State Chem.* **2001**, *156*, 452.

(31) Kucharczyk, B.; Zabrzeski, J. Monolithic $La_{1-x}Pt_xMnO_3$ and $LaMn_{1-x}Pt_xO_3$ Perovskite Catalysts for the Oxidation of Methane and Carbon Oxide. *Environ. Prot. Eng.* **2008**, *34* (4), 75.

(32) Rivera, A.; León, C.; Santamaria, J.; Várez, A.; V'yunov, O.; Belous, A. G.; Alonso, J. A.; Sanz, J. Percolation-Limited Ionic Diffusion in $Li_{0.5-x}Na_xLa_{0.5}TiO_3$ perovskites ($0 \leq x \leq 0.5$). *Chem. Mater.* **2002**, *14*, 5148.

(33) Muktha, B.; Madras, G.; Guru Row, T. N. A novel scheelite-like structure of $BaBi_2Mo_4O_{16}$: Photocatalysis and Investigation of the Solid Solution, $BaBi_2Mo_{4-x}W_xO_{16}$ ($0.25 \leq x \leq 1$). *J. Photochem. Photobiol. A* **2006**, *187*, 177.

(34) Muktha, B.; Aarthi, T.; Madras, G.; Guru Row, T. N. Substitution Effect on the Photocatalytic Degradation by the Series $A_xBi_{26-x}Mo_{10}O_{68+0.5y}$ (A = Ba, $y = 0$; A = Bi, La, $y = 2$): A Kinetic Study. *J. Phys. Chem. B.* **2006**, *110*, 10280.

(35) Mahapatra, S.; Nayak, S. K.; Madras, G.; Guru Row, T. N. Microwave Synthesis and Photocatalytic Activity of Nano Lanthanide (Ce, Pr and Nd) Orthovanadates. *Ind. Eng. Chem. Res.* **2008**, *47*, 6509.

(36) Tang, J.; Zou, Z.; Katagiri, M.; Kako, T.; Ye, J. Photocatalytic Degradation of MB on MIn_2O_4 (M = alkali earth metal) under Visible Light: Effects of Crystal and Electronic Structure on the Photocatalytic Activity. *Catal. Today.* **2004**, *93*−*95*, 885.

(37) Ding, J.; Sun, S.; Bao, J.; Luo, Z.; Gao, C. Synthesis of $CaIn_2O_4$ Rods and Its Photocatalytic Performance Under Visible-light Irradiation. *Catal. Lett.* **2009**, *130*, 147.

(38) Xie, B.; Zhang, H.; Cai, P.; Qiu, R.; Xiong, Y. Simultaneous Photocatalytic Reduction of Cr(VI) and Oxidation of Phenol over Monoclinic $BiVO_4$ under Visible Light Irradiation. *Chemosphere* **2006**, *63*, 956.

(39) Mahapatra, S.; Madras, G.; Guru Row, T. N. Structural and Photocatalytic Activity of Lanthanide (Ce, Pr, and Nd) Molybdovanadates. *J. Phys. Chem. C* **2007**, *111*, 6505.

Received for review April 17, 2009
Revised manuscript received June 26, 2009
Accepted June 28, 2009

IE9006134